Heme−Peptide Models for Hemoproteins. 2. *N*-Acetylmicroperoxidase-8: Study of the $\pi-\pi$ Dimers Formed at High Ionic Strength Using a Modified Version of Molecular Exciton Theory

Orde Q. Munro*[,1a] and Helder M. Marques[1b]

Centre for Molecular Design, Department of Chemistry, University of the Witwatersrand, Wits 2050, Johannesburg, South Africa

Received March 8, 1995[⊗]

AcMP8 is the Cys-14-acetylated water-soluble heme−octapeptide fragment obtained proteolytically from cytochrome *c*. Two successive dimerization equilibria are observed with increasing ionic strength in aqueous solution at neutral pH (part 1, preceding article). The electronic spectra of the two $\pi-\pi$ dimers were extracted from the absorption envelopes at 2.01 and 4.02 M ionic strength and resolved by Gaussian analysis. The principal transitions were assigned using a tailored version of molecular exciton theory based on coupling of the main *x*- and *y*-polarized transition dipole moments of the interacting heme groups. The spectra of both $\pi-\pi$ dimers indicate that the *y*-polarized exciton states are *blue*-shifted relative to the excited states of the monomer, while the *x*-polarized exciton states exhibit a *red* shift. These shifts were correctly predicted by a simple dipole−dipole coupling model. From an analysis of the resultant transition dipole moments to the exciton states with $B_x(0,0)$ and $B_y(0,0)$ character and the magnitudes of their red and blue exciton shifts, respectively, we have determined the dipole−dipole interaction geometries for both dimers. The principal difference between the interaction geometry in the first dimer and that in the second is a stronger interaction for the *y*-polarized transition dipoles and somewhat weakened interaction for the *x*-polarized transition dipoles. From an analysis of available crystallographic data for porphyrin and metalloporphyrin $\pi-\pi$ dimers (Scheidt, W. R.; Lee, Y. J. *Struct. Bonding* **1987**, *64*, 1) and the results of our exciton model, we conclude that the origin of the coordinate system for the Soret transition dipole moments of AcMP8 is not metal-centered. Furthermore, since the true directions of the *x*- and *y*-axes of the low-symmetry heme chromophore in AcMP8 are unknown, we have not been able to determine the structures of the $\pi-\pi$ dimers from a knowledge of their transition dipole−dipole interaction geometries. This study therefore highlights one of the shortfalls of molecular exciton theory.

Introduction

Microperoxidase-8 (MP8[1c]) is the water-soluble heme−octapeptide fragment obtained proteolytically from cytochrome *c*. Acetylation of the N-terminal amino group of the polypeptide chain covalently attached to the heme group affords AcMP8.[2−6] Although the proximal ligand of the parent cytochrome, His-18, is retained in AcMP8 (Figure 1), the cytochrome sequence containing the *trans* ligand, Met-80, is removed during hydrolysis to leave the sixth coordination site occupied by water.[2] AcMP8 is therefore a useful biomimetic model system for myoglobin, hemoglobin, and the peroxidase enzymes.

EPR,[3,7a] Mössbauer,[7a,b] and magnetic[7c] studies on ferric AcMP8 have shown that the spin state of the metal is temperature- and ligand-dependent, as might be expected for an iron(III) porphyrin axially coordinated by histidine and water at pH 7 (HHis−Fe^{3+}−OH_2).[2] However, the pH-dependent forms of AcMP8 are unusual in that they exhibit thermal spin equilibria between predominantly high-spin (>78% $S = {}^5/_2$) quantum-mechanically admixed intermediate-spin ($S = {}^3/_2, {}^5/_2$) states and low-spin ($S = {}^1/_2$) states, in contrast to the familiar $S = {}^5/_2 \rightleftarrows S = {}^1/_2$ equilibria of hemoglobin,[8] myoglobin,[9] and

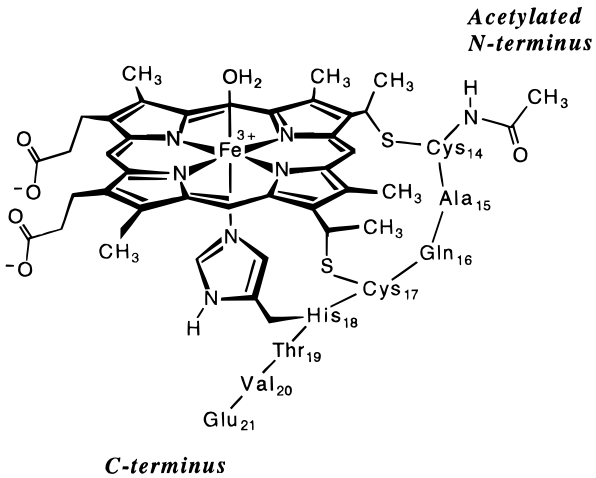

Figure 1. Structure of the water-soluble heme peptide *N*-acetylmicroperoxidase-8. The appended polypeptide chain is numbered according to the amino acid sequence in cytochrome *c*.

⊗ Abstract published in *Advance ACS Abstracts,* May 1, 1996.

(1) (a) Current address: Department of Chemistry and Biochemistry, University of Notre Dame, Notre Dame, IN 46556. Electronic mail: munro.1@nd.edu. (b) Electronic mail: hmarques@aurum.chem.wits.ac.za. (c) Abbreviations: AcMP8, *N*-acetylmicroperoxidase-8; CD, circular dichroism; Ct, center; L, general label for ligand donor atom; LS, lateral shift; M, methyl group; Mb, myoglobin; MOPS, 3-morpholinopropanesulfonic acid; MP11, microperoxidase-11; MP8, microperoxidase-8; MPS, mean plane separation; P, propionate group; SA, slip angle; SR, thioether substituent.

(2) Part 1: Munro, O. Q.; Marques, H. M. *Inorg. Chem.* **1996**, *35*, 0000.
(3) Yang, E. K.; Sauer, K. In *Electron Transport and Oxygen Utilization*; Ho, C., Ed.; Elsevier: North Holland: Amsterdam, 1982; p 82.
(4) Wang, J.-S.; Baek, H. K.; Van Wart, H. E. *Biochem. Biophys. Res. Commun.* **1991**, *179*, 1320.
(5) Wang, J.-S.; Tsai, A.-L.; Heldt, J.; Palmer, G.; Van Wart, H. E. *J. Biol. Chem.* **1992**, *267*, 15310.
(6) Wang, J.-S.; Van Wart, H. E. *J. Phys. Chem.* **1989**, *93*, 7925.
(7) (a) Part 3: Munro, O. Q.; Marques, H. M.; Pollak, H.; van Wyk, J. Manuscript in preparation. (b) Munro, O. Q.; Marques, H. M.; Pollak, H.; Malas, N. *Nucl. Instrum. Methods* **1993**, *B76*, 315. (c) Part 4: Munro, O. Q.; Marques, H. M.; de Wet, M.; Hill, H. A. O.; Battle, P. D. Manuscript in preparation.
(8) Iizuka, T.; Kotani, M. *Biochim. Biophys. Acta* **1969**, *194*, 351.
(9) Iizuka, T.; Kotani, M. *Biochim. Biophys. Acta* **1969**, *181*, 275.

S0020-1669(95)00285-0 CCC: $12.00

cytochrome *c* peroxidase.[10,11] Indeed, although AcMP8 is *six-coordinate* at pH 7,[2] therefore attaining a maximum of 22% $S = {}^3/_2$ character,[7a] it is one of the few monohistidine-bound ferric porphyrin systems that comes close to modeling the quantum-mechanically admixed intermediate-spin ground states of the five-coordinate ferricytochromes *c*′,[12−16] which manifest between 37 and 63% $S = {}^3/_2$ character.[14,15]

In part 1[2] of this study, we observed two dimerization equilibria in aqueous solutions of AcMP8 with increasing ionic strength. Our model fitting the data assumed that the first equilibrium resulted in the formation of a negatively-charged dimer, D_1^{4-}, while the second equilibrium favored the formation of a neutral dimer, D_2^0. NMR studies on MP11,[17] the related heme−undecapeptide fragment from cytochrome *c*, have shown that the distal face of the molecule is more accessible to solvent than the proximal face since the appended polypeptide chain adopts a coiled α-helical conformation beneath the His-18 binding site. Such a conformation is also likely for AcMP8 (Figure 1). We suspect that a strong $\pi-\pi$ interaction between the exposed distal faces of the interacting monomers in the first dimer is destabilized by electrostatic repulsion, leading to a relatively weak complex. The second dimer formed at higher ionic strength, however, appears to be uncharged and therefore somewhat more tightly packed. Furthermore, the spectroscopic changes attending dimerization of AcMP8 were inconsistent with intermolecular coordination,[2] reflecting protection of the α-NH_2 group of Cys-14, which, in addition to $\pi-\pi$ complexation between heme groups, has previously been implicated in the mechanism of aggregation of MP8 in aqueous solution.[18,19] It is therefore likely that the AcMP8 dimers formed at high ionic strength are face-to-face $\pi-\pi$ complexes similar in structure to the dimers formed by other porphyrins,[20−22] metalloporphyrins,[21,23−29] and chlorins.[30]

The only definitive method for structurally characterizing these dimeric systems is, of course, X-ray crystallography.[31] However, this requires single crystals suitable for X-ray work, and these are not easily obtained when the complex is highly asymmetric. Moreover, $\pi-\pi$ complexes that are dimeric in solution may not crystallize as dimers, or may crystallize with a significantly different geometry. Fortunately, the solution structures of porphyrin and metalloporphyrin dimers can be partly determined using ^{13}C and ^1H NMR spectroscopy.[27−30] Although several approximations have to be made in order to arrive at a suitable geometry for the interacting monomers, one of the advantages of this technique is that the pyrrole rings involved in the overlap interaction can be identified.

Electronic spectroscopy is by far the most common method used to detect porphyrin and metalloporphyrin $\pi-\pi$ complexes in solution[18−26,32] but, unlike NMR spectroscopy, less readily affords information about the stereochemistry of the interaction. Spectra obtained from metalloporphyrin[33] and phthalocyanin[34,35] films assembled on surfaces, however, have been analyzed using molecular exciton theory,[36−42] which is based on geometry-dependent electrostatic coupling of the principal transition dipoles of the chromophores that are in contact with one another. Angle-resolved absorption measurements give the most information about the stereochemistry of the chromophore−chromophore interaction,[33,35] but such measurements are restricted to systems containing chromophores anchored on surfaces or to studies on single crystals. An alternative strategy involves the synthesis of covalently and coordinatively linked dimers in which the relative orientations of the porphyrins are restricted to a limited set of conformations.[43−46] Analysis of the spectrum of the monomer followed by that of the dimer affords solutions to the geometry-dependent terms describing the exciton interaction between the main transition dipoles and thus information about the stereochemistry of the dimer.

However, one drawback of molecular exciton theory is that it cannot be used to pinpoint exactly where the transition dipoles lie within the interacting chromophores. This is rarely appreciated, and as shown in this study, it is not always correct to assume that the principal transition dipole moments will be positioned at the center of a large chromophore like a porphyrin. The upshot of this is that it is difficult to establish which pyrrole rings of a porphyrin or metalloporphyrin overlap in the dimer. The information obtained using exciton theory is therefore less

(10) Iizuka, T.; Kotani, M.; Yonetani, T. *Biochim. Biophys. Acta* **1968**, *167*, 257.
(11) Iizuka, T.; Yonetani, T. *Adv. Biophys.* **1970**, *1*, 157.
(12) Weber, P. C.; Howard, A.; Xuong, N. H.; Salemme, F. R. *J. Mol. Biol.* **1981**, *153*, 399.
(13) Finzel, B. C.; Weber, P. C.; Hardman, K. D.; Salemme, F. R. *J. Mol. Biol.* **1985**, *186*, 627.
(14) Maltempo, M. M. *J. Chem. Phys.* **1974**, *61*, 2540.
(15) Maltempo, M. M.; Moss, T. H. *Q. Rev. Biophys.* **1976**, *9*, 181.
(16) Moore, G. R.; Pettigrew, G. W. *Cytochromes c. Evolutionary, Structural and Physicochemical Aspects*; Springer-Verlag: New York, 1990.
(17) Kimura, K.; Peterson, J.; Wilson, M.; Cookson, D. J.; Williams, R. J. P. *J. Inorg. Biochem.* **1981**, *15*, 11.
(18) Aron, J.; Baldwin, D. A.; Marques, H. M.; Pratt, J. M.; Adams, P. A. *J. Inorg. Biochem.*, **1986**, *27*, 227−243.
(19) Urry, D. W.; Pettegrew, J. W. *J. Am. Chem. Soc.* **1967**, *89*, 5276.
(20) Pasternack, R. F.; Huber, P. R.; Boyd, P.; Engasser, G.; Francesconi, L.; Gibbs, E.; Fasella, P.; Venturo, G. C.; de Hinds, L. C. *J. Am. Chem. Soc.* **1972**, *94*, 4511.
(21) White, W. I. In *The Porphyrins*; Dolphin, D., Ed.; Academic Press: New York, 1978; Vol. V, Chapter 7, p 303.
(22) (a) Abraham, R. J.; Burbidge, P. A.; Jackson, A. H.; Macdonald, D. B. *J. Chem. Soc. B* **1966**, 620. (b) Janson, T. R.; Katz, J. J. *J. Magn. Reson.* **1972**, *6*, 209.
(23) Pasternack, R. F. *Ann. N.Y. Acad. Sci.* **1973**, *206*, 614.
(24) Caughey, W. S.; Eberspaecher, H.; Fuchsman, W. H.; McCoy, S.; Alben, J. O. *Ann. N.Y. Acad. Sci.* **1968**, *153*, 722.
(25) Gallagher, W. A.; Elliott, W. B. *Biochem. J.* **1968**, *108*, 131.
(26) (a) Shelnutt, J. A.; Dobry, M. M.; Satterlee, J. D. *J. Phys. Chem.* **1984**, *88*, 4980. (b) Shelnutt, J. A. *J. Phys. Chem.* **1984**, *88*, 4988.
(27) (a) Abraham, R. J.; Eivazi, F.; Pearson, H.; Smith, K. M. *J. Chem. Soc., Chem. Commun.* **1976**, 698. (b) Abraham, R. J.; Eivazi, F.; Pearson, H.; Smith, K. M. *J. Chem. Soc., Chem. Commun.* **1976**, 699. (c) Abraham, R. J.; Barnett, G. H.; Hawkes, G. E.; Smith, K. M. *Tetrahedron* **1976**, *32*, 2949. (d) Abraham, R. J.; Evans, B.; Smith, K. M. *Tetrahedron* **1978**, *34*, 1213.
(28) Snyder, R. V.; La Mar, G. N. *J. Am. Chem. Soc.* **1977**, *99*, 7178.
(29) (a) La Mar, G. N.; Viscio, D. B. *J. Am. Chem. Soc.* **1974**, *96*, 7354. (b) La Mar, G. N.; Viscio, D. B.; Smith, K. M.; Caughey, W. S.; Smith, M. L. *J. Am. Chem. Soc.* **1978**, *100*, 8085. (c) Viscio, D. B.; La Mar, G. N. *J. Am. Chem. Soc.* **1978**, *100*, 8092. (d) Viscio, D. B.; La Mar, G. N. *J. Am. Chem. Soc.* **1978**, *100*, 8096.
(30) (a) Closs, G. L.; Katz, J. J.; Pennington, F. C.; Thomas, M. R.; Strain, H. H. *J. Am. Chem. Soc.* **1963**, *85*, 3809. (b) Mazumdar, S.; Mitra, S. *J. Phys. Chem.* **1990**, *94*, 561.
(31) Scheidt, W. R.; Lee, Y. J. *Struct. Bonding* **1987**, *64*, 1.
(32) Mukudan, N. E.; Pethö, G.; Dixon, D. W.; Kim, M. S.; Marzilli, L. G. *Inorg. Chem.* **1994**, *33*, 4676.
(33) Schick, G. A.; Schreiman, I. C.; Wagner, R. W.; Lindsey, J. S.; Bocian, D. F. *J. Am. Chem. Soc.* **1989**, *111*, 1344.
(34) Sharp, J. H.; Lardon, M. *J. Phys. Chem.* **1968**, *72*, 3231.
(35) Kobayashi, N.; Lam, H.; Nevin, W. A.; Janda, P.; Leznoff, C. C.; Koyama, T.; Monden, A.; Shirai, H. *J. Am. Chem. Soc.* **1994**, *116*, 879.
(36) Kasha, M.; Rawls, H. R.; El-Bayoumi, M. A. *Pure Appl. Chem.* **1965**, *11*, 371.
(37) Kasha, M. *Radiat. Res.* **1963**, *20*, 55.
(38) McRae, E. G.; Kasha, M. *J. Chem. Phys.* **1958**, *28*, 721.
(39) Fulton, R. L.; Gouterman, M. *J. Chem. Phys.* **1961**, *35*, 1059.
(40) Fulton, R. L.; Gouterman, M. *J. Chem. Phys.* **1961**, *41*, 2280.
(41) Shipman, L. L.; Norris, J. R.; Katz, J. J. *J. Phys. Chem.* **1976**, *80*, 877.
(42) Knox, R. S. *J. Phys. Chem.* **1994**, *98*, 7270.
(43) Osuka, A.; Maruyama, K. *J. Am. Chem. Soc.* **1988**, *110*, 4454.
(44) Nagata, T.; Osuka, A.; Maruyama, K. *J. Am. Chem. Soc.* **1990**, *112*, 3054.
(45) Kobuke, Y.; Miyaji, H. *J. Am. Chem. Soc.* **1994**, *116*, 4111.
(46) Anderson, H. L. *Inorg. Chem.* **1994**, *33*, 972.

exact than that from an NMR study. Moreover, there are other assumptions that have to be made in order to reduce the problem, which has three unknown angular parameters after exciton shifts and transition dipoles have been acquired from analysis of the spectra, to something that can be handled in the fewest unknowns. The method can at best afford an approximate structure for a dimeric system in solution, particularly when the dimers are not covalently linked but are held together by dispersion forces.[19,47]

In this study, we have used the species distribution of AcMP8[2] to extract the spectral envelopes of the dimers from the electronic spectra measured at 2.01 and 4.02 M ionic strength. The principal bands fitting the spectrum of the monomer, M, the first dimer, D_1^{4-}, and the second dimer, D_2^0, have been assigned and the band energies and transition dipole moments used in a tailored version of molecular exciton theory to afford some structural information about the relative orientations of the interacting monomers.

Materials and Methods

AcMP8 was prepared as described previously.[2] Separate solutions of AcMP8, each with [AcMP8] = 5.1 μM and buffered at pH 7.00 with 1.0 mM MOPS, were prepared using sodium perchlorate monohydrate (Merck) to adjust the total ionic strength from 0.10 to 4.02 M. Spectra were collected at 25.0 ± 0.2 °C using a Cary 1E UV−visible spectrophotometer with a wavelength accuracy of ±0.2 nm; the data capture interval was 0.08 nm.

At μ = 0.1 M, the fraction of monomeric AcMP8 is 1.00 and the absorption spectrum therefore corresponds to that of the monomer, M (Figure 4b, part 1).[2] The spectrum of the monomer (440−300 nm) was fitted to a sum of five Gaussian bands (eq 1) using standard

$$A_T = \sum_{j=1}^{5} \alpha_j \exp\left[\frac{-(\lambda - \lambda_j)^2}{2\Delta_j^2}\right] \quad (1)$$

nonlinear curve-fitting procedures, where A_T is the total absorbance, λ the measured wavelength, λ_j the wavelength at which the jth Gaussian component reaches a maximum absorbance, α_j the intensity of the jth peak, and Δ_j the half-width of the jth band at 0.607 of the maximum intensity. One of the Gaussian components of eq 1 was used to fit the broad, low-intensity UV background, and the remaining four were used to fit the principal transitions constituting the absorption envelope.

At μ = 2.01 M, the fractions of the AcMP8 monomer, M, and the first dimer, D_1^{4-}, are about 0.8 and 0.2, respectively (Figure 4b, part 1).[2] Subtraction of the spectrum of the monomer scaled by ∼0.8 from the absorption envelope at μ = 2.01 M should give the absorption envelope of the first dimer. We found in fact that subtraction of the monomer spectrum scaled by 0.73 afforded a positive difference spectrum representing the absorption envelope of the first dimer. The difference spectrum was then fitted to the sum of seven Gaussian components. Two of the seven components, at the wavelength extrema of the envelope, were used to fit the irregular background, while the remaining five were used to fit the principal transitions between 300 and 440 nm.

At μ = 4.02 M, the solution comprises about 40% M, 20% D_1^{4-}, and 40% D_2^0 (Figure 4b, part 1).[2] Subtraction of the absorption envelope of the monomer scaled by 0.4 and the difference spectrum obtained at μ = 2.01 M, which represents the spectral contribution due to the first dimer (about 20%), from the spectrum at μ = 4.02 M afforded the absorption spectrum of the second dimer, D_2^0. The resulting envelope was fitted as before to the sum of seven Gaussian components.

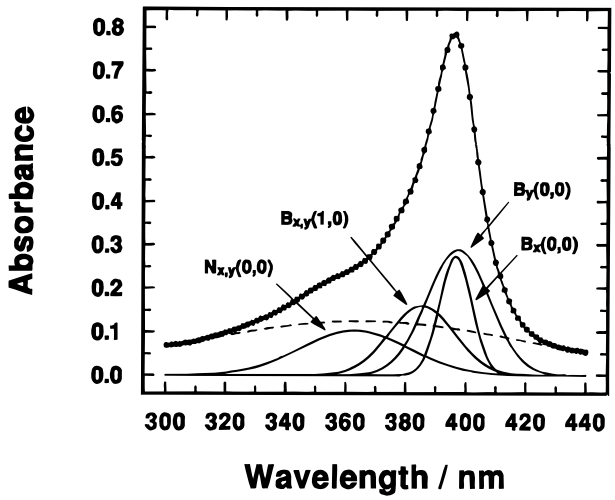

Figure 2. Resolved electronic absorption spectrum of 5.1 μM AcMP8 at a total ionic strength of 0.10 M ($NaClO_4$) at pH 7.00 and 25 °C. The solution comprises monomeric AcMP8 at this ionic strength. The principal transitions were assigned on the basis of the assigned spectrum of metMb·H_2O.[49] One broad Gaussian band was used to fit the parabolic absorption background (dotted line).

Results

The four principal Gaussian bands fitting the absorption envelope of monomeric AcMP8 at an ionic strength of 0.10 M are shown in Figure 2. The values of λ_j and Δ_j obtained from fitting the spectroscopic data to eq 1 are listed in Table 1. Since we chose to fit the absorption data as a function of wavelength, the refined parameters of eq 1 (Table 1) were converted into energies in wavenumbers for calculation of the remaining data. (Figure S1, Supporting Information, shows that the same results are obtained whether the absorbance data are fitted as a function of wavenumber in cm^{-1} or wavelength in nm.) The molar absorptivity of the jth band, ϵ_j, was calculated from the fitted value of α_j using Beer's law, while the integrated area of the jth band, Ω_j, was calculated using eq 2. The integrated

$$\Omega_j = (\epsilon_j/\mathrm{cm^2\ mmol^{-1}})(\Delta_j/\mathrm{cm^{-1}})(2\pi)^{1/2} \quad (2)$$

absorption coefficient, ξ_j, oscillator strength, f_j, transition dipole moment between final and initial states, $|\mu^{fi}_j|$, and dipole length for the jth band were calculated using standard methods.[50]

The inset to Figure 3 shows a plot of the difference spectrum obtained by subtracting the near-UV envelope of monomeric AcMP8 (μ = 0.10 M) scaled by 0.73 from the absorption spectrum recorded at an ionic strength of 2.01 M. The difference spectrum corresponds to the absorption envelope of the first $\pi-\pi$ dimer, D_1^{4-}, whose fractional abundance is ∼0.2 at this ionic strength.[2,51] The principal Gaussian bands fitting the difference spectrum and their assignments are given in the main part of Figure 3, while the parameters derived from fitting the data to eq 1 are listed in Table 1.

The fractions of the monomer (0.4) and the first dimer (0.27) were used in conjunction with their absorption envelopes to obtain the spectrum of the second dimer from the UV spectrum

(47) Sauer, K.; Lindsay Smith, J. R.; Schultz, A. J. *J. Am. Chem. Soc.* **1966**, *88*, 2681.
(48) Goff, H. M. In *Iron Porphyrins, Part 1*; Lever, A. B. P., Gray, H. B., Eds.; Physical Bioinorganic Chemistry Series; Addison-Wesley: Reading, MA, 1983; p 237.
(49) Makinen, M. W.; Churg, A. K. In *Iron Porphyrins, Part 1*; Lever, A. B. P., Gray, H. B., Eds.; Physical Bioinorganic Chemistry Series; Addison-Wesley: Reading, MA, 1983; p 141.
(50) Atkins, P. W. *Physical Chemistry*, 3rd ed.; Oxford University Press: Oxford, 1986; Chapter 19, p 463.
(51) The fractional abundance of a particular species, e.g., the first $\pi-\pi$ dimer, is the fraction of the total chromophore units in the sample that are present as that species.

Table 1. Resolution of the UV Spectrum of AcMP8 into Constituent Gaussian Bands at Selected Ionic Strengths (pH 7.0, 25 °C)[a]

μ	λ_j[b]	Δ_j	ϵ_j	Ω_j	ξ_j	f_j	$\lvert\mu^{fi}_j\rvert$	$\lvert\mu^{fi}_j\rvert$[c]	η_j
0.10	363.1	1369(26)	2.01(1)	6.9(2)	2.1(1)	0.298(7)	1.6(3)	4.8(8)	1.0(2)
	385.5	734(18)	3.13(0_4)	5.8(2)	1.7(1)	0.249(7)	1.5(3)	4.5(8)	0.9(2)
	396.7	343(33)	5.35(1)	4.6(5)	1.4(1)	0.20(2)	1.4(4)	4.1(1.3)	0.9(3)
	397.5	665(19)	5.65(0_4)	9.4(3)	2.8(1)	0.41(1)	2.0(3)	5.9(1.0)	1.2(2)
2.01	335.5	1703(36)	7.30(3)	31.2(8)	9.4(2)	1.35(4)	3.3(5)	9.8(1.6)	2.0(3)
	356.8	944(32)	12.7(1)	30(1)	9.0(4)	1.30(5)	3.3(7)	9.9(2.0)	2.1(4)
	371.2	705(27)	13.7(1)	24(1)	7.3(3)	1.04(5)	3.0(7)	9.1(2.0)	1.9(4)
	384.1	393(27)	5.90(4)	5.8(4)	1.7(1)	0.25(2)	1.5(4)	4.5(1.2)	0.9(3)
	409.5	436(22)	4.05(3)	4.4(3)	1.3(1)	0.19(1)	1.4(3)	4.1(1.0)	0.8(2)
4.02	336.6	1531(36)	2.10(3)	8.1(3)	2.4(1)	0.35(1)	1.7(3)	5.0(1.0)	1.0(2)
	359.8	1278(31)	4.52(3)	14.5(4)	4.4(1)	0.63(2)	2.3(4)	6.9(1.1)	1.4(2)
	369.6	1038(33)	6.80(3)	17.7(6)	5.3(2)	0.76(3)	2.6(5)	7.7(1.4)	1.6(3)
	387.2	427(25)	1.40(2)	1.5(1)	0.45(3)	0.065(5)	0.8(2)	2.3(6)	0.5(1)
	408.0	782(24)	2.35(1)	4.6(2)	1.4(1)	0.199(7)	1.4(3)	4.2(8)	0.9(2)

[a] The esd's of the least significant digits are given in parentheses. Symbols and units: μ, ionic strength/M; for the jth band, λ_j, wavelength of the band maximum/nm; Δ_j, half-bandwidth at 0.607 of the maximum height/cm^{-1}; ϵ_j, molar absorptivity at $\lambda_j/10^4$ cm^2 mmol^{-1}; Ω_j, integrated area/10^7 cm mmol^{-1}; ξ_j, integrated absorption coefficient/10^{18} cm^2 mmol^{-1} s^{-1}; f_j, oscillator strength; $|\mu^{fi}_j|$, transition dipole moment/10^{-29} C m; η_j, dipole length/Å. [b] All wavelengths are accurate to ±0.2 nm. [c] Transition dipole moment in D.

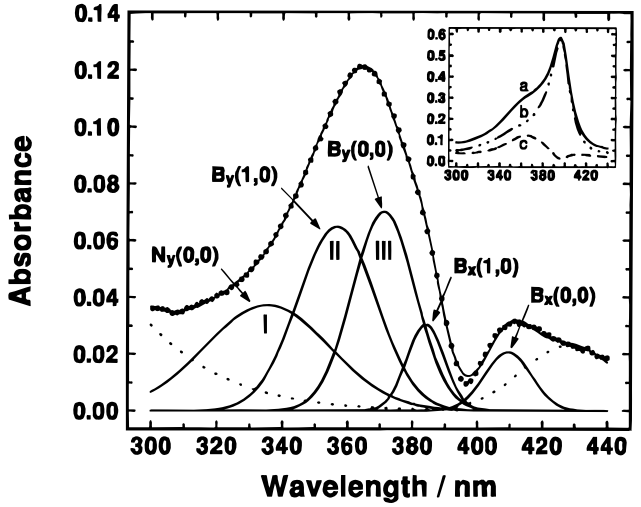

Figure 3. Plot of (a) the total absorption envelope obtained from a 5.1 μM solution of AcMP8 at an ionic strength of 2.01 M (pH 7.00, 25 °C), (b) the envelope of the monomer from Figure 2 scaled by 0.73, (c) the difference spectrum corresponding to the absorption envelope of the first AcMP8 $\pi-\pi$ dimer (inset), and, in the main diagram, the resolved spectrum of the dimer. The irregular absorption background at the extrema of the difference envelope was fitted using Gaussian-shaped bands (dotted lines). The principal transitions were assigned using exciton theory (see text) which adequately accounts for the observed splitting and shifts of the orthogonally polarized exciton states.

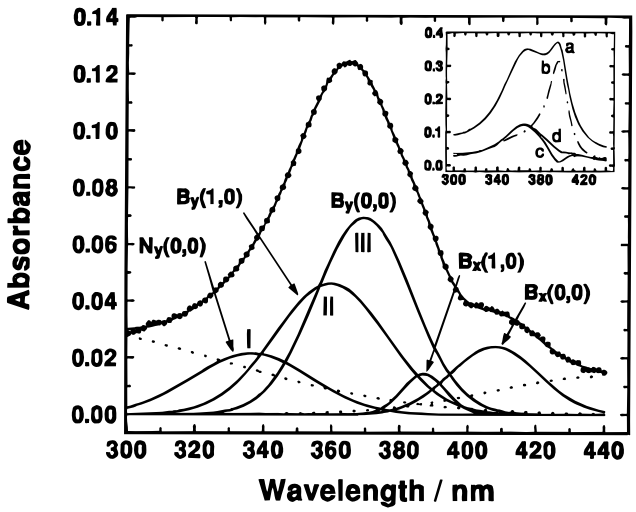

Figure 4. Plot of (a) the total absorption envelope obtained from a 5.1 μM solution of AcMP8 at an ionic strength of 4.02 M (pH 7.00, 25 °C), (b) the envelope of the monomer from Figure 2 scaled by 0.40, (c) the envelope of the first dimer having a fractional abundance of ca. 0.2 from Figure 3, (d) the difference spectrum (a − b − c) corresponding to the absorption envelope of the second AcMP8 $\pi-\pi$ dimer (inset), and, in the main diagram, the resolved spectrum of the dimer. The irregular absorption background at the extrema of the difference envelope was fitted using Gaussian-shaped bands (dotted lines). The exciton bands of the dimer, derived from the principal bands of monomeric AcMP8, were assigned using exciton theory (see text).

of AcMP8 at $\mu = 4.02$ M. The contributions from each of the three species present at this ionic strength are shown in the inset to Figure 4. The main part of Figure 4 displays the resolved absorption spectrum of D_2^0 with band assignments. Spectroscopic data calculated from the principal Gaussian bands fitting the absorption spectrum are listed in Table 1.

Correlation matrices for the parameters of eq 1 fitting the data in Figures 2−4 are given in Tables S1−S3 (Supporting Information). As expected for closely-spaced Gaussian bands, some of the parameters exhibit a high degree of cross-correlation. For example, the height and half-width at 0.607 of the maximum intensity of the $B_y(0,0)$ band in Figure 2, α_5 and Δ_5 in eq 1, have high *negative* correlations with α_2, λ_2, and Δ_2 (Table S1). This indicates that a reduction in intensity and blue shift in the maximum of the $N_{x,y}(0,0)$ component would lead to larger values of α_5 and Δ_5, i.e., that the $B_y(0,0)$ component would compensate for any loss of intensity in the N band component. Since λ_5 shows high *positive* correlations with α_2, λ_2, and Δ_2 (Table S1), a loss of intensity and blue shift of the $N_{x,y}(0,0)$ component would be accompanied by a compensating blue shift of the $B_y(0,0)$ component. These results suggest that parameters derived from the Gaussian components fitting the spectra in Figures 2−4 may exhibit some inaccuracies as a result of such cross-correlations. Unfortunately, this is an unavoidable consequence of using nonlinear least-squares numerical techniques to resolve spectra of this complexity.

Discussion

Transition Assignments: Monomeric AcMP8. The previously established[2] axial ligand combination of ferric AcMP8 at pH 7.0, H_2O and His-18, favors a predominantly $S = {}^5/_2$ state, which is a signature of a ligand field environment similar to that found in metMb···H_2O. The assigned solution and polarized single-crystal spectra of metMb[49] may therefore be used to assign the principal transitions in the electronic spectrum of AcMP8. In high-spin iron(III) porphyrins of axial, or near-axial symmetry, the Soret band at ca. 392−400 nm arises from the $\pi \rightarrow \pi^*$ transition to the doubly degenerate x,y-polarized

B(0,0) state.[52] The transition occurs at a slightly longer wavelength (ca. 408−414 nm) in high-spin ferric hemoproteins, such as metMb and the peroxidases,[53] and may be split into its components depending on the nature of the axial ligands and, to a lesser extent, the porphyrin substitution pattern.[52,54] We found that two nonequivalent Gaussian components at 396.7 and 397.5 nm (Figure 2, Table 1) were the *minimum* number required to fit the Soret region of the spectrum of monomeric AcMP8 at pH 7. This suggests that the low symmetry of the heme group (C_1) splits the degenerate state into its two components, $B_x(0,0)$ and $B_y(0,0)$. The separation between these states is quite small, amounting to 51 cm^{-1}, and is well within the range (25−300 cm^{-1}) predicted from the polarization ratio spectrum of sperm-whale metMb.[49] The polarizations of these bands have been arbitrarily assigned (Figure 2) since their true polarization can only be established from single-crystal measurements.[49] Differentiation of the components of the Soret band, even if arbitrary, is necessary at this stage since the exciton shifts of the *x*- and *y*-polarized transitions are apparently opposite in the spectra of the AcMP8 $\pi-\pi$ dimers (*vide infra*). The transition dipole moments of the Soret components are clearly inequivalent (Table 1), but this is not unexpected in systems of lower than D_{4h} symmetry, for example, protoporphyrin IX and heme *c* derivatives, porphyrin free bases,[55] and reduced porphyrin species.[56]

We have assigned the Gaussian band at 385.5 nm (Figure 2, Table 1) to the vibronic transition to the B(1,0) state. In axially symmetric heme systems, this transition exhibits *x*,*y*-polarization and is degenerate.[49] Since the B state in AcMP8 at pH 7 is not degenerate, splitting of the vibronic satellite is also expected, although overlap with the $B_y(0,0)$ band and a lower absorption intensity appears to render any likely splitting unresolvable. An approximate value for the vibrational quantum separating the B(0,0) and B(1,0) states in monomeric AcMP8 may be calculated by assuming degeneracy of the B(0,0) state and subtracting the mean energy of its two components from that of the B(1,0) state. This gives a value of 758 cm^{-1}, which is about half as large as that found for metMb···H_2O (1400 cm^{-1}),[49] suggesting that the heme group in AcMP8 is probably somewhat more flexible than the protein-bound heme group of metMb due to greater rotational freedom of the axial histidine and fewer stabilizing polypeptide−heme nonbonded interactions.

The *x*,*y*-polarized transition to the nearly degenerate N state in metMb···H_2O is observed as a broad shoulder at 357 nm in the solution and single-crystal spectra of the protein.[49] The broad Gaussian band reaching a maximum at 363.1 nm in the fitted spectrum of AcMP8 (Figure 2) is therefore assigned to a transition to a nearly degenerate N state of the heme peptide. Although it may be possible to fit the 360 nm region of the spectrum with two Gaussian components to demonstrate the likely splitting of this state, this is not a necessary condition for fitting the data and we therefore conclude that splitting of the N state in AcMP8 is probably slight.

Transition Assignments: The First $\pi-\pi$ Dimer. At an ionic strength of 2.01 M, 20% of the sample exists as the first $\pi-\pi$ dimer (cf. part 1, Figure 4b).[2] The difference spectrum shown in Figure 3 is fitted by five principal Gaussian bands and corresponds to the absorption envelope of the dimer. The

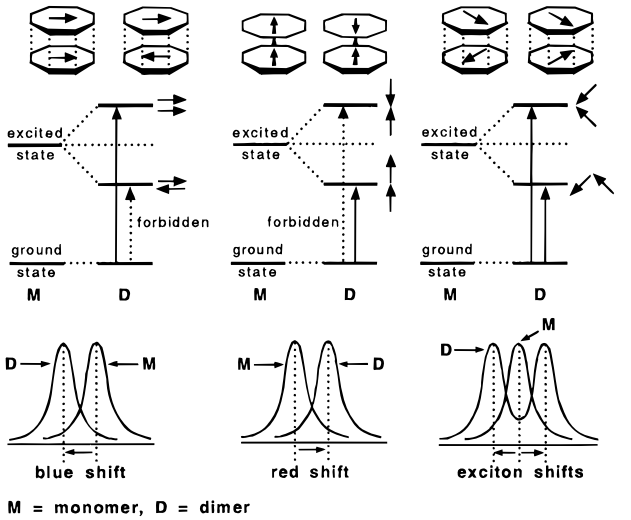

Figure 5. Diagram depicting the exciton states that arise from the coupling of transition dipoles in electronically interacting chromophores with various geometries. The idealized spectra of the dimeric systems are shown relative to the monomer but do not reflect changes in intensity which may accompany transitions to the exciton states.

subtraction procedure is likely to introduce some errors in the spectroscopic parameters calculated from the Gaussian bands (Table 1), particularly around 400 nm where the inset to Figure 3 indicates that the difference between the monomer spectrum and the total spectrum is almost zero. Nevertheless, in contrast to the spectrum of monomeric AcMP8, it is clear that at least two additional transitions contribute to the observed spectrum of the first $\pi-\pi$ dimer. Any model accounting for the spectrum of the dimer must therefore explain two observations: (i) that there are three intense transitions below 380 nm and (ii) that two weaker transitions appear in the 380−420 nm region of the spectrum. (There may be additional weak transitions that remain unresolved as a result of overlap with the more prominent transitions in this region.)

Molecular exciton theory may be used both qualitatively and quantitatively to account for the spectra of dimers and higher aggregates of interacting planar chromophores such as the nucleotide bases of DNA,[57,58] aromatic dyes,[38,59,60] porphyrins,[33,43−46] phthalocyanins,[34,35] and chlorins.[41,42,47] The essence of the theory[36−42] is that the principal plane-polarized transition dipole moments of the interacting chromophores couple electrostatically under the influence of the electric field of an incident photon of the correct frequency. Since the photon wavelength is much longer than the distance separating the dipoles, simultaneous excitation of the chromophores that comprise the molecular aggregate occurs. If one considers a pair of interacting transition dipoles in a dimer (Figure 5), then excitation of a parallel arrangement of the dipoles leads to a higher energy exciton state and a corresponding *blue* shift in the energy of the band relative to the case of the monomer. Excitation of an antiparallel pair would lead to a *red*-shifted lower-energy exciton state; however, such a state is forbidden and so the transition is absent from the spectrum.[36,37] This is the case most frequently encountered in $\pi-\pi$ dimers in which the planes of the monomers lie parallel to one another. However, if the two monomers are covalently linked and are coplanar (Figure 5), then the transition dipoles of the two units

(52) Gouterman, M. *J. Chem. Phys.* **1959**, *30*, 1139.
(53) Smith, D. W.; Williams, R. J. P. *Struct. Bonding* **1970**, *7*, 1.
(54) Loew, G. H. In *Iron Porphyrins, Part 1*; Lever, A. B. P., Gray, H. B., Eds.; Physical Bioinorganic Chemistry Series; Addison-Wesley: Reading, MA, 1983; p 1.
(55) Gouterman, M. *J. Mol. Spectrosc.* **1961**, *6*, 138.
(56) Gouterman, M.; Wagnière, G. H.; Snyder, L. C. *J. Mol. Spectrosc.* **1963**, *11*, 108.
(57) Rhodes, W. *J. Am. Chem. Soc.* **1961**, *83*, 3609.
(58) Tinoco, I., Jr. *J. Am. Chem. Soc.* **1960**, *82*, 4785.
(59) Levinson, G. S.; Simpson, W. T.; Curtis, W. *J. Am. Chem. Soc.* **1957**, *79*, 4314.
(60) Emerson, E. S.; Conlin, M. A.; Rosenoff, A. E.; Norland, K. S.; Rodriguez, H.; Chin, D.; Bird, G. R. *J. Phys. Chem.* **1967**, *71*, 2396.

may take on head-to-tail or head-to-head relative orientations. The former leads to an allowed, low-energy exciton state, and the latter, to a forbidden, high-energy exciton state.[36,37] In coplanar systems, transition dipoles orthogonal to these may be aligned parallel or antiparallel to one another, and this simply leads to a situation analogous to the first. A third possibility that exists applies to π-stacked and covalently-linked chromophores. An oblique arrangement for an interacting pair of transition dipoles will have a resultant moment whether the dipoles are in a nearly head-to-head or a nearly head-to-tail configuration. Allowed lower-energy and higher-energy exciton states are therefore possible, and the spectrum of the dimer may resemble a split spectrum of the monomer if both configurations arise. Red- or blue-shifted exciton states may also result from oblique coupling of the transition dipole moments if either a nearly head-to-tail (red shift) or a nearly head-to-head (blue shift) interaction geometry is favored. Thus, the electronic interaction between chromophores within a dimer or aggregate may lead to changes in the intensity and energy of transitions in the dimer spectrum relative to those observed in the monomer spectrum. The type of spectrum obtained for a dimeric system will therefore be critically dependent upon the exact geometry of the interaction.

In effect, all of the above possibilities can be thought of as excitation of the resultant of the interacting transition dipoles of the two monomers, and the problem may be treated algebraically as one of vector addition, where the vectors being added are the transition dipoles in the two interacting monomers. While this should enable prediction of the geometry of the interaction from the resultant transition dipoles measured from the exciton bands in the spectrum of the dimer, the energies of the dipole−dipole interactions, and hence the exciton shifts of the dimer bands, must be treated using a distance- and geometry-dependent electrostatic coupling model.[61−63] This is the two-pronged approach that we have attempted to use to delineate the interaction between the B_x and B_y dipoles of each heme group in the two types of $\pi-\pi$ dimer formed by AcMP8 (*vide infra*).

In Figure 3, the three more intense bands, I, II, and III, closely resemble the N, B(1,0), and B(0,0) bands of the monomer shown in Figure 2. However, each clearly exhibits a *blue* shift of ca. 26−30 nm. If it is assumed that one of the components, e.g. the *y*-component, of each of the three main transitions of the monomer is more intense than the *x*-component, as might be inferred from the anisotropy of the B(0,0) components (Figure 2), then the three more intense components fitting the absorption envelope of the $\pi-\pi$ dimer below 380 nm in Figure 3 are due to transitions to the exciton states with mainly $N_y(0,0)$ (335.5 nm), $B_y(1,0)$ (356.8 nm), and $B_y(0,0)$ (371.2 nm) character. The validity of such an assignment can be confirmed by noting that the spacing between these exciton bands closely matches that between the fitted components of the monomer spectrum in Figure 2.[64] Whether these exciton bands truly exhibit *y*-polarization or not could only be answered in a single-crystal polarization study.

The obvious question that follows is, what happens to the transitions to the corresponding *x*-polarized exciton states? Since the $B_x(0,0)$ component of the monomer spectrum is much weaker than the $B_y(0,0)$ component (Figure 2), all the *x*-components of the main bands in the electronic spectrum of the monomer are likely to have lower oscillator strengths than the corresponding *y*-components. The shift in wavelength of an exciton band relative to the wavelength of the corresponding band of the monomer depends on the magnitude of the interacting transition dipoles, as well as their orientation (*vide infra*).[42] Weak transition dipoles, even when interacting maximally, should not lead to very large exciton shifts, and one would therefore expect the transitions to the *x*-polarized exciton states of the dimer to lie closer in energy to the transitions of the monomer.

Since the *x*-polarized dipoles will be orthogonal to the *y*-polarized dipoles, and the latter interact to produce *blue-shifted* exciton states in the dimer (indicating either a parallel or an oblique dipole−dipole configuration), the *x*-polarized exciton states can either be higher or lower in energy than the corresponding excited states of the monomer. The fact that one distinct but relatively weak transition is found above 400 nm in Figure 3 suggests that the weaker *x*-polarized transitions of the monomer interact in an oblique manner to produce *red-shifted* exciton bands. If we assume that the longest-wavelength transition at 409.5 nm (Table 1) corresponds to the *x*-polarized transition to the exciton state with mainly $B_x(0,0)$ character, then the observation that the red shift (ca. 13 nm) to this state is about half the blue shift to the $B_y(0,0)$ exciton state is in accord with the fact that the exciton shift depends on the magnitude of the interacting transition dipoles. While we cannot be sure that the red-shifted band at 409.5 nm actually corresponds to the transition to the $B_x(0,0)$ exciton state, a very similar band with a nearly equal oscillator strength is found in the spectrum of the second $\pi-\pi$ dimer at 408 nm (*vide infra*), arguing that the second dimer is similar in structure to the first and that this band cannot be spurious. Furthermore, while the broad Gaussian band at ∼420 nm used to fit the irregular background in Figure 3 might be confused with a transition in this region, it is clear from Figure 4 that the band is actually fitting background intensity.

If the transition at 409.5 nm in Figure 3 is to the $B_x(0,0)$ exciton state of the dimer, then a vibronic transition to the $B_x(1,0)$ exciton state must be found 11−25 nm to the blue of this band. This is indeed the case, since a band of comparable oscillator strength is found at 384.1 nm in Figure 3. It is interesting to note that the vibrational quantum separating the $B_y(0,0)$ and $B_y(1,0)$ exciton states (1087 cm^{-1}) is somewhat larger than that separating these states in the monomer (783 cm^{-1}). The same is true for the *x*-polarized exciton states, where the separation is 1615 cm^{-1}. The magnitudes of these quanta are not inconsistent with that found for metMb···H_2O (1400 cm^{-1}),[49] suggesting that the heme groups in the first AcMP8 dimer are conformationally about as flexible as the heme group in this protein and somewhat more constrained than the single heme group of monomeric AcMP8.

The $N_y(0,0)$ exciton state occurs ca. 21 nm to the blue of the $B_y(1,0)$ state and ca. 36 nm to the blue of the $B_y(0,0)$ state in Figure 3. If the transition at 409.5 nm in Figure 3 corresponds to excitation to the $B_x(0,0)$ exciton state of the $\pi-\pi$ dimer, then the transition to the $N_x(0,0)$ state should occur at about 36 nm to the blue of this band, i.e., at approximately 373 nm. However, this is a region in which the more prominent transitions to the *y*-polarized exciton states are strongly overlapped, and it is therefore likely that the $B_y(0,0)$ band and red tail of the $B_y(1,0)$ band fit the weak intensity expected from the transition to the $N_x(0,0)$ state.

(61) Dense, J. B. *Mathematical Techniques in Chemistry*; Wiley-Interscience: New York, 1975; Chapter 6, p 361.
(62) Atkins, P. W. *Physical Chemistry*, 4th ed.; Oxford University Press: Oxford, U.K., 1990; Chapter 22, pp 644−662.
(63) Laidler, K. J.; Meiser, J. H. *Physical Chemistry*; Benjamin/Cummings Publishing Co.: Menlo Park, CA, 1982; Chapter 16, p 754.
(64) The three prominent bands below 380 nm in Figure 3 are separated by ca. 15 (III−II) and 21 nm (II−I); the B(0,0)−B(1,0) and B(1,0)−N band spacings in monomeric AcMP8 (Figure 2) are ca. 12 and 22 nm, respectively.

Quantitative Aspects: A Simple Dipole−Dipole Coupling Model. Having assigned the main transitions in the spectrum of the monomer and first $\pi-\pi$ dimer, we then used exciton theory to gain a more quantitative picture of the dipole−dipole coupling that leads to the observed spectrum of this dimer. In particular, the model had to (i) account for the different intensities of the transitions to the *x*- and *y*-polarized exciton states and (ii) predict the red and blue shifts of the *x*- and *y*-polarized states, respectively.

If it is assumed that the most likely way of forming a $\pi-\pi$ dimer between two AcMP8 molecules involves a face-to-face dispersion interaction, then only the sterically unhindered faces of the hemes may interact. Furthermore, if it is assumed that the complex is formed by overlap of a pyrrole ring of one monomer with that of a second, then the two heme groups will be related by a C_2 axis parallel to the planes of the overlapping pyrrole rings and passing through the space between them. This type of $\pi-\pi$ interaction between porphyrins and metalloporphyrins is in fact common both in solution[29] and in the solid state.[31] One consequence of the geometry of such an interaction is that if an arbitrary set of Cartesian axes is placed in the framework of the first heme group, then the same axes of the second heme group will be related to those of the first by the C_2 operation. If we then define the C_2 axis as being equivalent to a 180° rotation about an axis parallel to the *y*-direction, the directions of the *x*- and *z*-axes in the second heme group will be the inverse of those in the first. Importantly, an *x*-polarized transition dipole of the second heme group will be oriented at ca. 180° relative to its direction in the first heme group within the frame of this definition.

Figure 6a is an illustration of this type of $\pi-\pi$ dimer where the two AcMP8 heme groups are related by a C_2 rotation axis. The dimer has been drawn by overlapping pyrrole ring III of heme 1 with pyrrole ring III of heme 2.[65] The geometry of the interaction is idealized with the *x*- and *y*-axes of each group arranged in a parallel manner.

To explain (i) the directions and magnitudes of the exciton shifts in the spectra of the AcMP8 $\pi-\pi$ dimers and (ii) the dipole strengths of the exciton bands, we have considered a vector-coupling model for the $B_x(0,0)$ and $B_y(0,0)$ transition dipoles of the monomer units comprising the dimer using the coordinate system shown in Figure 6b. This model clearly depends on a highly specific (C_2) interaction geometry for the two sets of transition dipoles and will therefore apply only to those systems with an analogous chromophore configuration. While such a model may not be completely general, it is nonetheless particularly useful for the analysis of dimers that comprise structurally asymmetric planar chromophore systems with only one accessible face. In Figure 6b, the nonequivalent, nondegenerate *x*- and *y*-polarized transition dipoles to the B(0,0) state of the first heme group are defined as lying along the Cartesian axes. The same transition dipoles of the second heme group are then placed at some other orientation in the shifted coordinate system, such that $\mu_{y(2)}$ makes an angle of φ with the

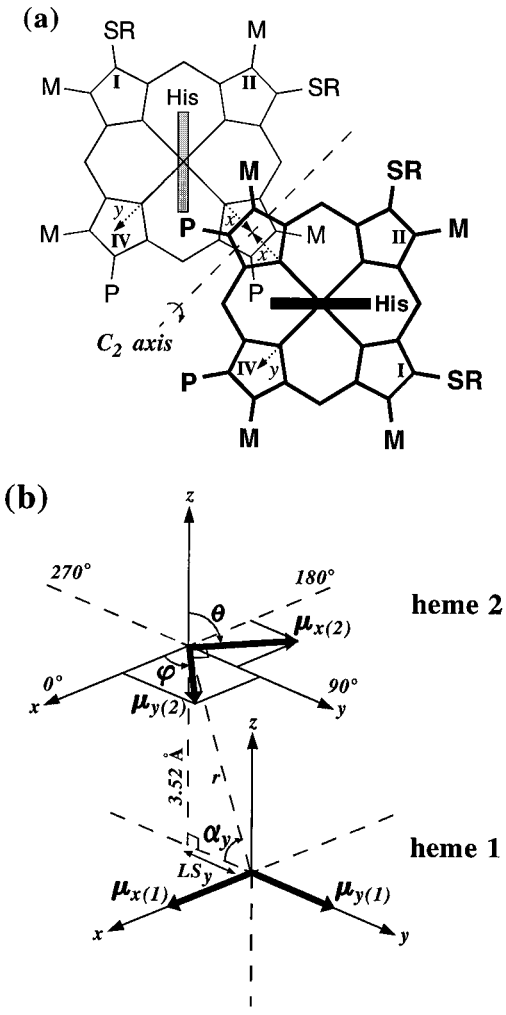

Figure 6. (a) Possible C_2 symmetry for the heme−heme interaction between two AcMP8 monomers showing the 2-fold axis and relationships between arbitrarily chosen *x*- and *y*-axes. The axial histidine is below the heme plane in the lower unit (thinner lines) and above the heme plane in the upper unit (thicker lines). Both hemes overlap at pyrrole ring III. (b) Coordinate systems and variables for the interactions between the $B_x(0,0)$ and $B_y(0,0)$ transition dipoles of the π-stacked heme groups. Note: the coordinate system for the dipoles does *not* necessarily coincide with that for the heme group in each case.

x-axis. ($\mu_{x(2)}$ will be located at $\varphi + 90°$ because of the formal C_2 symmetry of the dimer.) The origins of these two local coordinate systems are related by a translation of 3.52 Å along the *z*-direction. This distance corresponds to the mean plane separation (MPS) between porphyrin, metalloporphyrin, and chlorin $\pi-\pi$ dimers found by Scheidt and Lee[31] and is the first of several assumed parameters for the heme−heme interaction in the AcMP8 $\pi-\pi$ dimers. In addition to a rotation of φ degrees about the *z*-axis, the dipoles may be tilted by an angle θ relative to the *z*-axis. Furthermore, the origins of the dipoles in the two heme groups may be translated or laterally-shifted along both the *x*- and *y*-directions. This introduces two additional angles, α_x and α_y. In each case, α is the angle between the line joining the centers of the transition dipoles and their *x*- or *y*-components. When $\alpha = 90°$, $r = 3.52$ Å and the center−center separation of the dipoles is equivalent to the MPS. It is important to note that the coordinate systems for the transition dipoles may *not* coincide with the coordinate systems defined by the $Fe-N_{porphyrin}$ and $Fe-L_{axial}$ directions of the heme groups. (We will show later that this is in fact the case.)

(65) (a) The III-on-III overlap geometry in Figure 6a is consistent with Smith and McLendon's ^{1}H NMR data on the six-coordinate $S = 1/2$ cyanide complex of MP8;[65b] the spectra recorded at 22 °C in D_2O show that the heme methyl groups at positions 3 and 5 (3-CH_3 and 5-CH_3) exhibit a downfield shift in resonant frequency upon dimerization of the monomers with increasing heme concentration. Moreover, the temperature dependence of the 5-CH_3 group resonance displays the greatest deviation from Curie law behavior. Due to dipolar relaxation effects, the heme methyl groups closest in space to the paramagnetic centers will show the greatest downfield shifts in the dimer.[28,29] The NMR data for MP8···CN^- therefore suggest formation of a dimer in which pyrrole ring III of one six-coordinate monomer overlaps with pyrrole ring III of the other. (b) Smith, M. C.; McLendon, G. *J. Am. Chem. Soc.* **1981**, *103*, 4912.

The simplest way to treat the problem is to look at the coupling of $\mu_{y(1)}$ in heme 1 with the resultant *y*-component arising from $\mu_{y(2)}$ and $\mu_{x(2)}$ in heme **2** (Figure 6b). This should give the sign and magnitude of the exciton shift to the $B_y(0,0)$ state of the $\pi-\pi$ dimer and the magnitude of the transition dipole of the exciton band as a function of φ, θ, and α_y. The magnitude of $\mu_{y(1)}$ (=$\mu_{y(2)}$) is known from the spectrum of the monomer, and the transition dipole of the $B_y(0,0)$ exciton band is known from the spectrum of the dimer (Table 1). The relative orientations of the transition dipoles in the heme groups can therefore be estimated from the measured exciton shift and the resultant *y*-polarized transition moment. The same argument applies to the *x*-polarized transition dipoles and exciton bands.

The standard equation[61−63] for calculating the potential energy of the dipole−dipole interaction is

$$E = \frac{\mu_1\mu_2\beta}{4\pi\epsilon_0\epsilon r^3} \tag{3}$$

where μ_1 and μ_2 are the magnitudes of dipoles 1 and 2, respectively, ϵ_0 the vacuum permittivity constant, ϵ the dielectric constant of the medium, and r the center-to-center separation of the dipoles. β is a geometry-dependent term which takes into account the relative orientations of the dipoles.

From Figure 6b, the change in energy of any *y*-polarized transition of the monomer upon formation of the dimer is given by eq 4, which can be rewritten as eq 5 and then as eq 6 if we

$$\Delta E = \frac{\mu_{y(1)}(\mu_{y(2)}\sin\theta\sin\varphi + \mu_{x(2)}\sin\theta\sin(\varphi+90))(1-3\cos^2\alpha_y)}{4\pi\epsilon_0\epsilon r^3} \tag{4}$$

impose the condition that the MPS must be 3.52 Å as observed in the solid state.[31] In eqs 5 and 6, $\gamma = \mu_{y(2)}\sin\theta\sin\varphi + \mu_{x(2)}$

$$\Delta\bar{\nu}/\mathrm{cm}^{-1} = \frac{4.523\times10^{32}\mu_{y(1)}\gamma(1-3\cos^2\alpha_y)}{(r/m)^3} \tag{5}$$

$$\Delta\bar{\nu}/\mathrm{cm}^{-1} = \frac{4.523\times10^{32}\mu_{y(1)}\gamma(1-3\cos^2\alpha_y)}{(3.52\times10^{-10}/\sin\alpha_y)^3} \tag{6}$$

$\sin\theta\sin(\varphi+90)$ and $\Delta\bar{\nu}$ is the shift in wavenumber of the *y*-polarized exciton band of the dimer relative to the *y*-polarized band of the monomer. The transition dipoles in eqs 5 and 6 are in C m and the angles in degrees. The exciton shift of an *x*-polarized band is given by eq 7, where $\eta = \mu_{y(2)}\sin\theta\cos\varphi$

$$\Delta\bar{\nu}/\mathrm{cm}^{-1} = \frac{4.523\times10^{32}\mu_{x(1)}\eta(1-3\cos^2\alpha_x)}{(3.52\times10^{-10}/\sin\alpha_x)^3} \tag{7}$$

$+\mu_{x(2)}\sin\theta\cos(\varphi+90)$ and the units are the same as before. Using standard[62] vector addition, the transition moments of the *y*- and *x*-polarized exciton bands are given by eqs 8 and 9, respectively.

$$\mu_{y\mathrm{T}} = (\mu_{y(1)}{}^2 + \gamma^2 + 2\mu_{y(1)}\gamma)^{1/2} \tag{8}$$

$$\mu_{x\mathrm{T}} = (\mu_{x(1)}{}^2 + \eta^2 + 2\mu_{x(1)}\eta)^{1/2} \tag{9}$$

In eqs 6 and 7, the scalar quantities $\mu_{y(1)}$ (=$\mu_{y(2)}$) and $\mu_{x(1)}$ (=$\mu_{x(2)}$) are known from experiment (Table 1), leaving the exciton shift dependent on three angular variables φ, θ, and α. The resultant transition moment of an exciton band, however, depends on only two unknowns, θ and φ (eqs 8 and 9), and with the reasonable assumption that $\theta = 90°$, i.e., that the heme groups are parallel, we can obtain an estimate of φ from a plot of $\mu_{y\mathrm{T}}$ or $\mu_{x\mathrm{T}}$ against φ and θ.

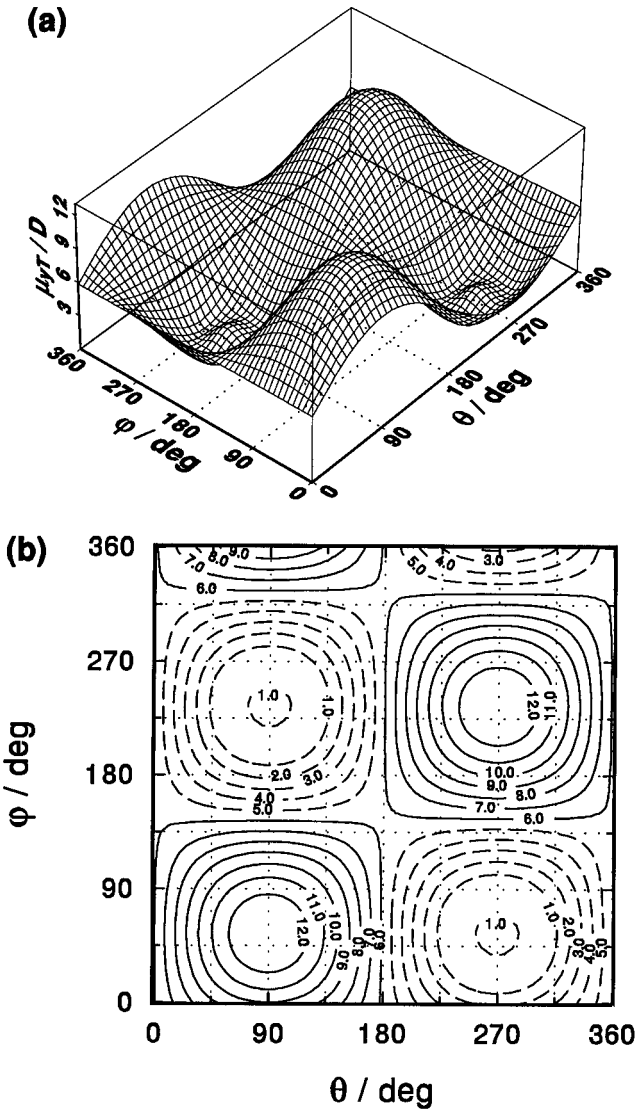

Figure 7. (a) Dependence of the resultant *y*-polarized transition dipole moment to the exciton state with $B_y(0,0)$ character on the orientation angles θ and φ (see Figure 6b). The resultant *y*-moment is nonvanishing in the regions at the bottoms of the wells due to *x*,*y*-coupling. (b) Map of the surface in part a. The resultant *y*-polarized dipole moment is in debyes. Both plots were generated from eq 8.

Figure 7a shows a surface plot of eq 8 with $\mu_{y(1)} = \mu_{y(2)} = 5.9$ D and $\mu_{x(1)} = \mu_{x(2)} = 4.1$ D (from Table 1). A contour map of the surface is displayed in Figure 7b. Both demonstrate how the intensity of the *y*-polarized transition to the $B_y(0,0)$ exciton state varies with the orientations of the two angles φ and θ. Equation 8 describes the coupling of the *y*-polarized transition dipole of heme 1 with the *y*-component of the *x*- and *y*-polarized transition dipoles of heme 2. In the absence of this "*x*,*y*-mixing" effect, the positions of the maxima and minima on the surface (not shown) are φ, $\theta = 90°$, 90° and 270°, 270° and φ, $\theta = 90°$, 270° and 270°, 90°, respectively. However, with *x*,*y*-mixing, the maxima shift to φ, $\theta = 56°$, 90° and 235°, 270°, and the minima become circular since two weaker maxima appear at the bottoms of the wells in these regions (Figure 7). These weaker maxima occur at φ, $\theta = 56°$, 270° and 235°, 90° and indicate that the transition moment integral of the *y*-

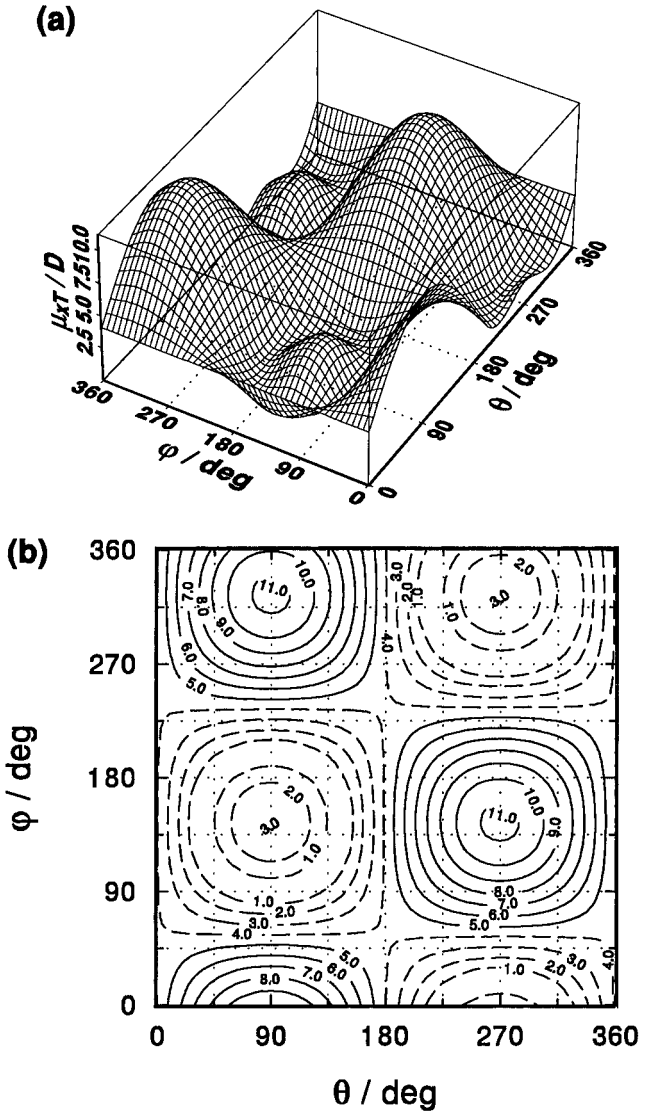

Figure 8. (a) Dependence of the resultant *x*-polarized transition dipole moment to the exciton state with $B_x(0,0)$ character on the orientation angles θ and φ (see Figure 6b). The resultant *x*-moment is nonvanishing in the regions at the bottoms of the wells due to *x*,*y*-coupling. (b) Map of the surface in part a. The resultant *x*-polarized dipole moment is in debyes. Both plots were generated from eq 9.

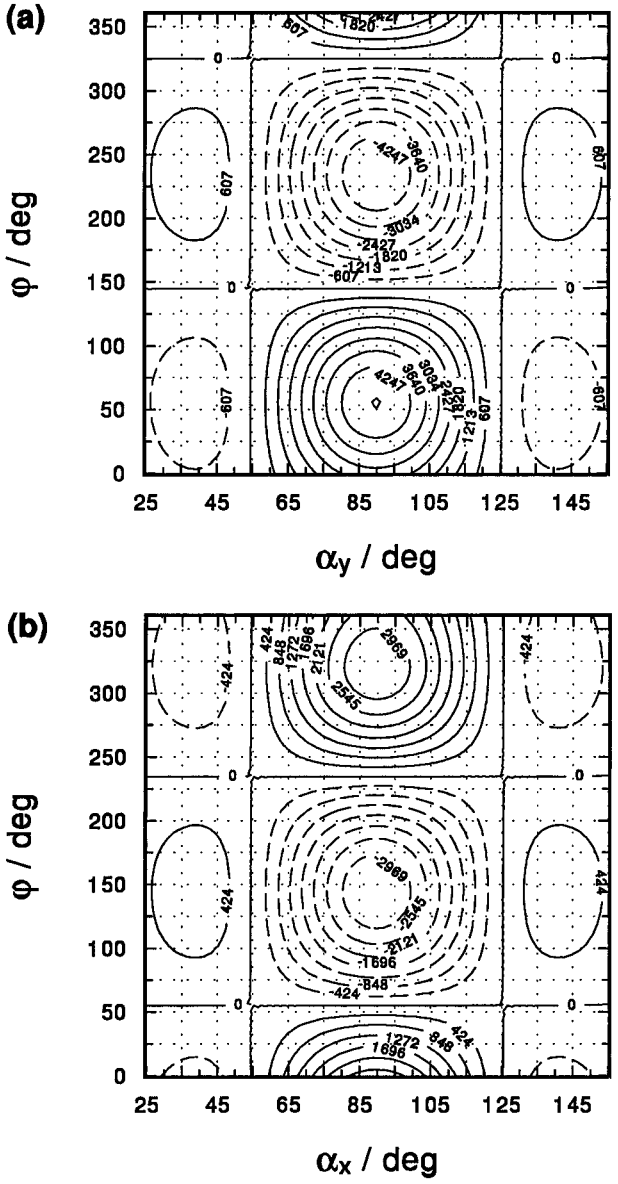

Figure 9. (a) Variation of the exciton shift of the $B_y(0,0)$ state, $\Delta\bar{\nu}$, in cm^{-1} with the angles φ and α_y of Figure 6b. The plot was generated from eq 6. The regions mapped by solid contours indicate a *blue* shift in transition energy relative to the monomer, while those mapped by dashed contours reflect a *red* shift. (b) The analogous plot of eq 7 for the transition to the $B_x(0,0)$ state.

polarized transition to the $B_y(0,0)$ exciton state for a dimer with this dipole−dipole orientation will be nonvanishing. In this case, the maximum is weak because the forbidden *y*-polarized transition is "stealing" intensity from the weaker *x*-polarized transition.

Figures 8 displays plots of eq 9 with $\mu_{y(1)} = \mu_{y(2)} = 5.9$ D and $\mu_{x(1)} = \mu_{x(2)} = 4.1$ D (from Table 1). Both plots show that the resultant *x*-polarized transition dipole moment is strongly dependent on the two angles θ and φ. In Figure 8a, the weaker pair of maxima on the surface are more intense than those in Figure 7a, reflecting the fact that the forbidden *x*-polarized transition to the exciton state with $B_x(0,0)$ character gains intensity in this region by mixing with the stronger *y*-polarized transition to the state with $B_y(0,0)$ character. In Figure 8b, the maximum and minimum values of the resultant *x*-polarized transition dipole moment are shifted relative to those of the *y*-polarized moment (Figure 7b). Because of this difference in phase, there are combinations of φ and θ that lead to a situation where the *y*-polarized exciton bands are of higher intensity than the *x*-polarized bands, in accord with the spectroscopic data in Figures 3 and 4.

The Structure of the First AcMP8 $\pi-\pi$ Dimer. If we make the reasonable assumption that the two heme groups are parallel in the $\pi-\pi$ dimer, $\theta = 90°$ in Figure 7b and the value of φ giving a resultant transition dipole moment of 9.1 D (Table 1) is ca. 118°. From Figure 8b, the resultant *x*-polarized transition dipole moment at the coordinate θ, $\varphi = 90°$, 118° is ca. 2.3 D. Considering that the errors in the magnitudes of $\mu_{y(1)}$ and $\mu_{x(2)}$ measured from the spectrum of the monomer (Table 1) are ca. 17 and 32%, respectively, and that these values are used in eqs 8 and 9 to generate the surfaces in Figures 7 and 8, the magnitude of the error in the estimate of the resultant *x*-polarized transition dipole moment will be about 36%. Comparison of the predicted resultant *x*-polarized transition dipole moment (2.3 ± 0.9 D, Figure 8b) with the observed value of 4.1 ± 1.0 D (Table 1) indicates that the agreement between theory and experiment is reasonable.

Figure 9 shows plots of eqs 6 and 7, respectively, with the value of θ fixed at 90° in each case (parallel heme groups). Figure 9a indicates that the exciton shift for the *y*-polarized

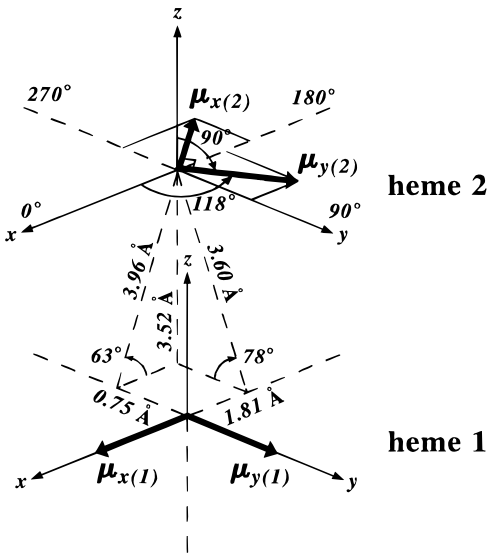

Figure 10. Geometry of the $B_x(0,0)$, $B_y(0,0)$ dipole−dipole interaction in the first AcMP8 $\pi-\pi$ dimer deduced using the spectroscopic data from the resolved electronic spectrum at 2.01 M ionic strength and a simple dipole−dipole coupling model.

transition is to the *blue* of the monomer band in a region bound by the magic angles $\alpha_y = 54.73°$ and $\alpha_y = 125.26°$ for $-34.23° < \varphi < 144.85°$ (solid contours). The exciton shift is to the *red* of the monomer band in the region with the boundaries $54.73° < \alpha_y < 125.26°$ and $144.85° < \varphi < 325.77°$ (dashed contours). Figure 9b reveals that the behavior of the transition to the *x*-polarized exciton state is similar but that the magnitudes of the maximum red and blue exciton shifts are smaller than those attainable by the *y*-polarized transition, reflecting coupling of the nonequivalent *x*- and *y*-polarized transitions to the B(0,0) state of the monomers comprising the dimer. Importantly, the combinations of φ and α_y that give a blue exciton shift in Figure 9a for the *y*-polarized transition may give either a blue or a red exciton shift for the *x*-polarized transition (Figure 9b).

Since the exciton shift of the $B_y(0,0)$ transition for the first dimer is 1782 cm^{-1} to the *blue* of the monomer band (Table 1), φ and α_y lie in the region mapped by the solid contours in Figure 9a. The value of φ determined from Figure 7 is 118°, and the value of α_y giving an exciton shift of 1782 cm^{-1} is therefore 78°. Furthermore, if $\varphi = 118°$, then from Figure 9b, eq 7 predicts that the exciton shift of the *x*-polarized transition will be to the *red* of the monomer transition. This prediction is in fact correct since the transition to the exciton state with $B_x(0,0)$ character is found 788 cm^{-1} to the *red* of the $B_x(0,0)$ band of the monomer (Table 1). Using this value for the exciton shift in Figure 9b with $\varphi = 118°$ gives $\alpha_x = 63°$. We now have all the data needed to construct a model of the dipole−dipole interaction in the first dimer since the *x* and *y* lateral shifts of the transition dipole centers and their center−center separation can be calculated from these angles, assuming of course an MPS of 3.52 Å (Figure 10).

The critical question is whether this information for the dipole−dipole interaction can be used to predict the geometry of the heme−heme interaction. If we were to assume that the centers of the two transition dipoles to the B(0,0) state in each monomer were located at the center of the chromophore, as is normal for centrosymmetric systems,[33,34,44−46] then as long as the *x*- and *y*-directions of the chromophore are known, the exact geometry of the heme−heme interaction could be determined because the transition dipoles would lie along these axes. In practice, the true *x*- and *y*-axes of the heme group and orientations of the transition dipoles can only be determined from a single-crystal polarization experiment.[66] Moreover, making the assumption that the transition dipoles have their centers at the center of the chromophore may only be correct when the heme group belongs to a high-symmetry point group. With low-symmetry systems like AcMP8 (C_1) there is no symmetry element that enforces such a condition, and as the following discussion shows, the $B_x(0,0)$ and $B_y(0,0)$ transition dipole moments do *not* have to be centered at the metal. It should also be clear that exciton theory cannot be used in this case to determine the geometry of the heme−heme interaction in the dimer.

Scheidt and Lee[31] have used four crystallographically determined geometrical parameters to classify the types of $\pi-\pi$ dimers formed by porphyrins and metalloporphyrins: (i) the mean plane separation (MPS) between the macrocyclic units; (ii) the center−center separation (Ct−Ct), which is roughly the metal−metal distance in metalloporphyrin dimers; (iii) the lateral shift (LS), which is the distance from one metal center to the point lying above the second metal center within the plane of the first porphyrin; and (iv) the slip angle (SA), which is the angle subtended at the metal center of one porphyrin by the vertical line to the porphyrin ring of the second unit and the line connecting the two metal centers.

We have plotted some of Scheidt and Lee's data[31] to determine the *empirical* relationships between lateral shift and center−center separation (Figure 11a), and between slip angle and lateral shift (Figure 11b) for $\pi-\pi$ dimers of porphyrins and metalloporphyrins of known structure. Figure 11a demonstrates that there is a monotonic increase in LS with Ct−Ct, while Figure 11b shows that the SA exhibits a monotonic increase with LS. Quadratic functions were assumed to fit the data and are given in the captions to these figures. If the transition dipoles to the B(0,0) state are centered at the metal in AcMP8, then the dipole−dipole lateral shifts along the *x*- and *y*-directions, center−center separations, and angles α_x and α_y in Figure 10 must match those that are typical for metalloporphyrin dimers of known structure.

Figure 11 may therefore be used to test whether the transition dipole moments are centered at the metal in AcMP8 or not. If we take the data for the B_y transition dipole moments from Figure 10 and use their center−center separation (3.60 Å) in the quadratic function fitting the data in Figure 11a, then the lateral shift should be 1.27 Å. Even though Scheidt and Lee's metal−metal lateral shifts are along no particular direction (*x* or *y*), it is clear that the B_y dipole−dipole lateral shift (0.75 Å, Figure 10) is too small for the dipoles to be centered at the metal. Otherwise, the dimer has the shortest LS described to date and is one of the tightest yet observed, which would be highly unlikely in the case of a six-coordinate complex such as AcMP8. This result suggests that the Soret transition dipole moments are more likely to be centered at the heme periphery (pyrrole rings and meso carbons) than at the metal in AcMP8.

If the dipole−dipole lateral shift (0.75 Å) is used in the empirical function fitting the data in Figure 11b, then a slip angle of 13.7° is predicted. This is in agreement with the slip angle of 12.0° (Figure 10) and suggests that a similar slip angle−lateral shift relationship holds for the transition dipole moments and the chromophore centers. However, this could be a fortuitous consequence of our assumption that the interplanar separation of the transition dipoles should be ca. 3.52 Å, which is the mean porphyrin plane separation observed in the solid state.[31] In fact, it might be argued that the MPS for dimers in

(66) Eaton, W. A.; Hofrichter, J. In *Methods in Enzymology*; Antonin, E., Rossi-Barnardi, L., Chiancone, E., Eds.; Academic Press: New York, 1981; Vol. 76, p 175.

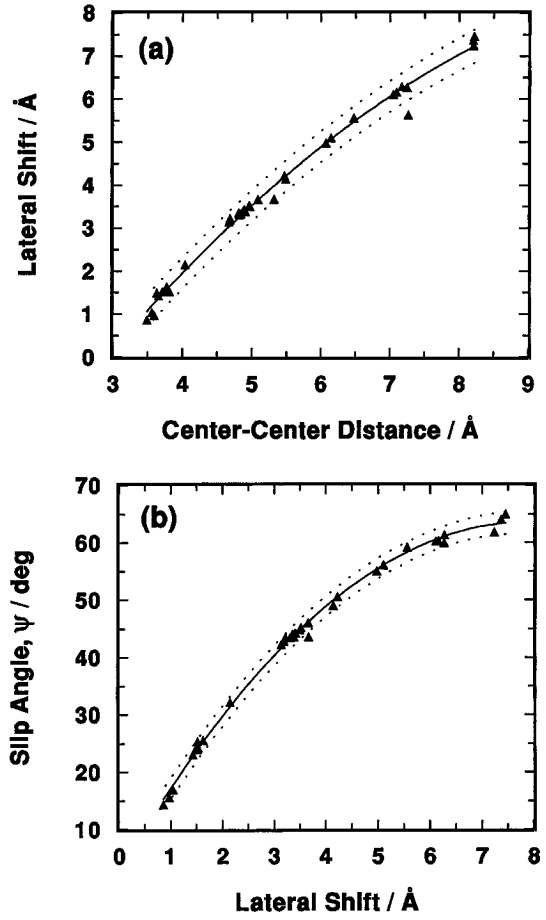

Figure 11. (a) Variation in the lateral shift between the centers of porphyrin and metalloporphyrin $\pi-\pi$ dimers with their center−center separation. The crystallographic data are from a review article by Scheidt and Lee.[31] The data were fitted to an *empirical* quadratic function (LS = $-6.3 \pm 0.5 + (2.5 \pm 0.2)$ (Ct−Ct) − (0.10 ± 0.01) (Ct−Ct)^2, $R^2 = 0.993$) to permit prediction of lateral shifts from measured center−center separations. The 95% confidence interval is shown. (b) Dependence of the slip angle on lateral shift for the above set of $\pi-\pi$ dimers of known geometry. The empirical quadratic function fitting the data (SA = $2.6 \pm 0.6 + (15.5 \pm 0.3)$ (LS) − (0.99 ± 0.04) (LS)^2, $R^2 = 0.997$) and 95% confidence interval are shown.

solution should be larger than the MPS observed in crystals since the heme groups are likely to be pushed apart by solvation effects.[29] Our exciton model can be used to predict the maximum separation of the heme groups in the dimer by assuming optimal dipole−dipole coupling and setting all angles in eq 5 to 90°. This gives $r \leq 4.7$ Å, which is shorter than the MPS found from NMR data for solvated dimers,[29] suggesting that the heme−heme interaction in AcMP8 is sufficiently strong to exclude solvent from the region between the heme planes.

Transition Assignments and Geometry of the Dipole−Dipole Interaction for the Second AcMP8 $\pi-\pi$ Dimer. Although the electronic spectrum of the second dimer (Figure 4) is very similar to that of the first, the spectroscopic data in Table 1 do indicate that there are small shifts in the energies of the principal transitions, suggesting a somewhat rearranged but overall similar structure for the second dimer. The transition assignments in Figure 4 are therefore the same as for the first dimer. The blue shift for the transition to the $B_y(0,0)$ exciton state is slightly larger for the second dimer (1899 cm^{-1}) than for the first (1782 cm^{-1}), while the red shift to the $B_x(0,0)$ exciton state in Figure 6 is marginally smaller (698 cm^{-1} *vs* 788 cm^{-1}). These shifts suggest a stronger dipole−dipole interaction along the *y*-direction and a weaker interaction along the *x*-direction.

Applying the previous arguments, we found that using the measured value of μ_{yT} (7.7 D, Table 1) in Figure 7b with $\theta = 90°$ gave $\varphi = 130°$ and that using these angular parameters in eq 9 gave $\mu_{xT} = 2.8 \pm 1.0$ D, which is within the uncertainty in the experimental value of 4.2 ± 0.8 D (Table 1). However, using the exciton shift of 1899 cm^{-1} with $\theta = 90°$ and $\varphi = 130°$ in eq 6 fails to give a solution for α_y. In fact, a solution for α_y can only be obtained if $\varphi \lesssim 121°$. The problem may well reflect an accumulation of data manipulation errors in extraction of the absorption envelope of the second dimer from the total spectrum recorded at this ionic strength or cross-correlation errors of the fitted Gaussian components. A solution is still possible, however, since taking the upper limit (9.1 D) of the value of μ_{yT} (7.7 ± 1.4 D) with $\theta = 90°$ gives $\varphi = 118°$ (Figure 7b) and $\alpha_y = 80°$ (eq 6), which is somewhat larger than α_y for the first dimer (78°). The value of α_x calculated from eq 7 is 62° and therefore marginally smaller than the value found for the first dimer (63°). These results are then in accord with the observed changes in Figure 4.

Within the limits of the model, it seems likely that the second dimer has a structure similar to that of the first, but with a shorter lateral shift along the *y*-direction and somewhat larger *x*-lateral shift.[67] This ultimately accounts for the larger blue shift to the $B_y(0,0)$ exciton state in the second dimer and probably explains why detection of the second equilibrium at high ionic strength is possible. A noteworthy caveat here is that this assumes that the coordinate systems for the principal transitions in the second dimer are unchanged relative to those in the first. Thus, as with the first, a definitive structure for the second $\pi-\pi$ dimer cannot be deduced from the geometry of the dipole−dipole interaction because the origins of the principal transitions relative to the axes of the heme group are unknown. Despite several attempts, we have been unable to crystallize AcMP8 from water or other solvent mixtures. Single-crystal spectroscopic studies, which would permit determination of the axis system of the heme group in AcMP8, therefore appear to be a remote possibility at this stage.

Finally, one might be tempted to study the dimerization reaction using both CD and absorption spectroscopy. Optical activity in the Soret region in heme-containing systems appears to arise from removal of the center of symmetry of the chromophore by mixed axial ligation of the metal or, in centrosymmetric systems, exciton coupling of the heme transition dipoles with transition dipoles of closely juxtaposed chromophores, e.g., aromatic amino acid side chains, amide carbonyl groups, or other heme groups.[68,69] In the latter case, the near-UV optical activity is a direct manifestation of the exciton interaction, and CD spectroscopy would be the method of choice for studying the physical behavior of such a system. However, the CD bands observed below 450 nm in the spectrum of monomeric MP8[19,70] and MP11[71] arise from the inherently

(67) (a) The dimer formed at high ionic strength is apparently similar in structure to the initial complex formed at low ionic strength. However, the origins of the transition dipole moments of the heme groups of the second dimer are laterally displaced relative to those of the first. This suggests that the second dimer is related to the first by slight displacement of one heme group relative to the other. Interestingly, this type of structural reorganization has been observed previously; Migita and La Mar's ^{1}H NMR study[67b] on the concentration-dependent oligomerization of derivatives of naturally occurring ferrous porphyrins in benzene-d_6 indicated that the dimers formed at higher concentrations were related to those formed at lower concentrations by translational displacement of the heme groups. (b) Migita, K.; La Mar, G. N. *J. Phys. Chem.* **1980**, *84*, 2953.

(68) Myer, Y. P.; Pande, A. In *The Porphyrins*; Dolphin, D., Ed.; Academic Press: New York, 1978; Vol. III, pp 271−322.

(69) Hsu, M.-C.; Woody, R. W. *J. Am. Chem. Soc.* **1971**, *93*, 3515.

(70) Myer, Y. P.; Harbury, H. A. *J. Biol. Chem.* **1966**, *241*, 4299.

low symmetry of these chromophores. While the exciton interactions established when two such intrinsically dissymmetric monomers interact may lead to a perturbation of the CD spectrum, they are not the primary source of the observed optical activity. CD spectroscopy is therefore unlikely to yield any additional information, over and above that obtainable by absorption spectroscopy, on the geometry of the heme−heme interaction in the present case.

Conclusions

AcMP8 forms two $\pi-\pi$ dimers in solution at high ionic strength that have similar near-UV absorption spectra. Analysis of the spectra within the framework of a tailored version of molecular exciton theory has permitted assignment of the principal transitions to the exciton states for both dimers. Furthermore, probable geometries for the dipole−dipole interactions within the stacked heme pairs have been deduced from the measured exciton shifts and resultant transition dipole moments of the dimer spectra. The geometries of the dipole−dipole interactions in the two dimers are similar, the main distinction being a difference in the center−center lateral shift along the *y*-direction. Even with an assumed C_2 symmetry for the dimer and heme−heme spacing of 3.52 Å, the model correctly predicts a blue shift in energy for the transition to the exciton state with $B_y(0,0)$ character and a red shift to the state with $B_x(0,0)$ character. The main shortfall of the method, however, is that, unless the actual *x*- and *y*-axes of the heme group are known, the geometry of the dipole−dipole interaction cannot be used to deduce the geometry of the heme−heme interaction. The most probable solution structures of the AcMP8 dimers therefore remain unknown.

Acknowledgment. H.M.M. thanks the University of the Witwatersrand, through the Centre for Molecular Design, and the Foundation for Research Development (FRD), Pretoria, for financial support. O.Q.M. thanks AECI Limited and the FRD for their past financial support in the form of postgraduate fellowships.

Supporting Information Available: Figure S1 (resolved electronic spectrum (as a function of wavenumber) of a 5.1 μM solution of AcMP8 at a total ionic strength of 0.10 M ($NaClO_4$) at pH 7.00 and 25 °C) and Tables S1−S3 (correlation matrices for the parameters of eq 1 (α_j, λ_j, and Δ_j) fitting the electronic spectra in Figures 2−4, respectively) (11 pages). Ordering information is given on any current masthead page.

IC950285U

(71) Urry, D. W. *J. Am. Chem. Soc.* **1967**, *89*, 4190.